

Aspects of Machian Gravity (II): Testing Theory against Rotation Curves of 175 SPARC Galaxies

Santanu Das

Theoretical Physics Group, Blackett Laboratory,
Imperial College London, SW7 2AZ, UK

E-mail: santanu.das@imperial.ac.uk

Abstract. Machian Gravity (MG) presents a mathematical framework that captures the essence of Mach's principle. It was formulated to address the limitations of general relativity and provide a gravity theory founded on robust logical principles. Unlike the approach of modifying existing theories by introducing extra scalar and vector degrees of freedom to account for observational data, MG offers a more coherent alternative. Previous investigations have revealed MG's potential to explain diverse phenomena, such as galactic velocity patterns, galaxy cluster mass distribution, and cosmic expansion, without requiring additional dark components in the universe. This study applies the MG acceleration law to a wide array of galaxies sourced from the SPARC galactic database. Through meticulous analysis, we have determined the optimal parameters of the Machian gravity model for each individual SPARC galaxy, consequently fitting their distinctive rotational profiles. Similar to the Modified Newtonian Dynamics (MOND), our results suggest the presence of an acceleration scale linked to galaxies, governing their rotational behavior near the outer regions. Importantly, this acceleration scale exhibits variability across different galaxies, albeit typically remaining around the order of 10^{-8}cm/s^2 .

Contents

1	Introduction	1
2	A brief discussion of Machian Gravity	2
2.1	Static, Spherically symmetric, Vacuum solution for weak gravitation field	3
3	A brief overview of SPARC galaxy database	5
4	Testing the theory against observations	7
5	Discussion and Conclusion	10

1 Introduction

The behavior of rotation curves in galaxies, as predicted by Newton’s gravitational theory, should exhibit a Keplerian fall-off in the orbital rotational speed v at the outer edge of the galaxy, given by $v^2 \propto M(r)/r$, where $M(r)$ represents the mass enclosed within the radius r . However, observations tell a different story. Instead of the anticipated decline, rotation curves tend to flatten out [1–4]. Contrary to expectations, velocities often increase towards the center of galaxies and then stabilize at around $v \sim 200 - 300$ km/s. On occasion, velocity might fall off or increase at a large radius while not complying with the Newtonian predictions. This inconsistency leads to a dynamic mass for galaxies that significantly surpasses their luminous mass.

This behavior of galactic rotation curves can be accounted for by introducing additional invisible matter or dark matter. This dark matter is presumed to exist in a spherical halo enveloping galaxies. The general consensus is that it consists of a cold, pressureless fluid. Their interaction with baryonic matter is extremely small but expected to be nonzero. Numerous candidates have been proposed to explain dark matter, with supersymmetric particles being a prominent contender [5]. However, the lack of experimental confirmation of such particles, especially from the Large Hadron Collider (LHC), strengthens alternative propositions such as axions and ultra-light scalar field dark matter, etc [6–16].

While dark matter may solve some of the velocity profiles, the evidence for dark matter relies on indirect observations. The observations only say that the baryonic matter that is present in a galaxy in the form of stars, neutral and high-temperature gas, etc., is not enough to provide sufficient gravity to explain the observed acceleration in these systems provided the calculations are made using the Newtonian law. Nevertheless, it’s plausible that the Newtonian mechanics that hold in laboratories and the solar system might not be directly applicable to galaxies. Adjusting the equations could potentially account for observed accelerations without invoking dark matter.

In recent years, a range of theories has emerged in attempts to explain dark matter. Empirical theories like Modified Newtonian Dynamics (MOND) have successfully matched galactic velocity profiles, though it violates the momentum conservation laws [17–20]. Consequently, a mathematically sound theory that can replicate the empirical achievements of MOND, may offer a plausible explanation for dark matter. Bekenstein proposed AQUA to provide a mathematical foundation to MOND [21–23]. Other theories, such as Modified Gravity STVG [28], Tensor-Vector-Scalar (TeVeS) theory [24–27], and Massive Gravity [29–32], have also emerged to reproduce galactic velocity profiles without requiring dark matter. Higher-dimensional concepts like Induced Matter Theory has also been proposed by researchers [33–37].

However, all of these theories are proposed to explain observed data rather than being derived from a foundational logical principle like general relativity. A robust theory should ideally be grounded in a strong logical or mathematical foundation. The inception of the general theory of relativity (GR) was initially intended to provide a mathematical formulation for Mach’s hypothesis. However, it became evident that GR did not align with Mach’s principle. Despite this, as GR successfully

accounted for various observations on the scale of the solar system, Einstein did not further attempt to reconcile this discrepancy or incorporate Mach’s argument into the theory.

In our previous work, we proposed a theory based on Mach’s principle to address the shortcomings of GR and provide an explanation for the inertia of objects. The theory, named as Machian Gravity (MG) is a five-dimensional theory. It can be derived from an action principle, thereby ensuring compliance with conservation principles. The fifth dimension, which we refer to as the background dimension, is intricately linked to the distribution of distant matter across the universe and plays a role in the inertia of particles. It has been demonstrated in [38] that MG converges towards GR in the context of the solar system, assuming all other matter is significantly distant. However, it deviates from GR on the galactic scale. Our earlier studies also illustrated how MG can provide insights into spiral galactic velocity profiles, galaxy cluster mass, and cosmic expansion history without necessitating extra dark components in the universe [38–40].

This paper undertakes a comprehensive analysis of the SPARC dataset using the Machian gravity model. The Spitzer Photometry and Accurate Rotation Curves (SPARC) dataset comprises observational data from 175 spiral galaxies, furnishing detailed insights into their rotation curves and other characteristics. Within this study, we employ MG to demonstrate how galactic rotational profiles can be accurately expounded using Machian gravity alone, obviating the necessity for additional nonbaryonic dark matter.

The structure of this paper is organized as follows. The second section briefly introduces the Machian gravity model and outlines its applicability in calculating galactic velocities. The third section provides a quick overview of the SPARC dataset. In the fourth section, we present our analysis of MG applied to the SPARC dataset. The final section encapsulates our conclusions and further discussion.

2 A brief discussion of Machian Gravity

The laws of physics should remain unchanged regardless of the choice of the coordinate system. While the general theory of relativity was proposed to satisfy this postulate, it ultimately diverges from this principle.

To illustrate the challenge posed by the general theory of relativity, let’s consider a thought experiment. The velocity and acceleration of a particle are relative quantities, necessitating a reference frame from which to measure them. Imagine there are only two point masses in the universe, with one being significantly heavier than the other. Let’s designate the heavier mass as A and the smaller mass as B, orbiting A in a circular path. We’ll examine two coordinate systems, both centered at A, with the z-axis perpendicular to B’s orbital plane. Suppose one of these coordinate systems is rotating with respect to the other at an angular velocity ω_z . Since there’s no distant object in the universe to establish the inertial coordinate system, we face ambiguity in distinguishing between the inertial and non-inertial coordinate systems. If we assume that the gravitational force is balanced by B’s centripetal acceleration, we need to know the angular velocity of B, which differs between the two reference frames. Consequently, the centripetal acceleration of B varies between these frames, rendering the measurement of gravitational acceleration impossible as there is no way to know the centrifugal acceleration.

In fact, if we align the x-axis of a reference frame with particle B, B will have no centripetal acceleration in that reference frame, leading to zero/undefined gravitational force on B in that frame. Since there are no distant matter (stars, or galaxies) in the universe except these two particles, the reference frames are equivalent. Therefore, the laws of physics should remain independent of the chosen reference frame, and the absence of centrifugal force in one frame should imply its absence in the other.

Einstein’s general theory of relativity explains acceleration using the curvature of the coordinate system. In cases like this, it becomes impossible to discern the acceleration or predict which coordinate will experience curvature and to what extent. Consider the example of Newton’s bucket, where two buckets filled with water rotate with respect to each other in the absence of other particles. Which bucket’s water surface will curve? If we attach coordinate frames to both buckets, one frame rotates concerning the other, and both coordinate systems are equivalent in the absence of distant matter.

If we assume curvature in one bucket's water surface, it implies different laws of physics in distinct reference frames, which is nonsensical.

Thus, we must assume that the laws of physics apply only in the presence of distant objects. The motion of these distant objects (stars, galaxies, etc.) creates a gravitational field in accelerating objects, giving rise to inertial forces such as centrifugal, Coriolis, and Euler forces etc. This concept was initially mathematically derived by Sciama and then studied by various authors [41–43]. In a 5-dimensional coordinate system, as we have demonstrated in [38], all these forces can be attributed to the motion of background stars and galaxies. The fifth dimension, denoted as the background dimension, is responsible for particle inertia.

2.1 Static, Spherically symmetric, Vacuum solution for weak gravitation field

The field equation describing MG is analogous to GR, but it operates in a five-dimensional space instead of the standard four dimensions. The five-dimensional line element can be represented as $ds^2 = \tilde{g}_{AB}dx^A dx^B$, where \tilde{g}_{AB} denotes the five-dimensional metric. Here, the indices A, B , etc., refer to the coordinates in the five-dimensional system, while Greek letters like α, β , etc., are reserved for the four-dimensional system. The notation $\tilde{\cdot}$ signifies quantities in the five-dimensional context.

When considering a vacuum, the field equation for MG becomes $\tilde{G}_{AB} = 0$, which upon manipulation can be expressed as $\tilde{R}_{AB} = 0$, where \tilde{R}_{AB} denotes the Ricci tensor. In the context of a weak gravitational field, the metric can be approximated as a perturbation over the Minkowski metric, written as $\tilde{g}_{AB} = \tilde{\eta}_{AB} + \tilde{\gamma}_{AB}$. Here, $\tilde{\eta}_{AB}$ is the Minkowski metric defined by $\tilde{\eta}_{AB} = \text{diag}(c^2, -1, -1, -1, -\frac{h^2}{4})$, and $\tilde{\gamma}_{AB}$ represents the metric perturbation.

For weak gravitational fields, the dominant component is the time component. Consequently, the 00 component of the Ricci tensor, $\tilde{R}_{00} = \tilde{R}_{0C0}^C$, simplifies to a form involving the Riemann tensor. The Riemann tensor can be expressed as:

$$\tilde{R}_{0A0}^B = \partial_A \tilde{\Gamma}_{00}^B - \partial_0 \tilde{\Gamma}_{A0}^B + \tilde{\Gamma}_{AC}^B \tilde{\Gamma}_{00}^C - \tilde{\Gamma}_{0C}^B \tilde{\Gamma}_{A0}^C. \quad (2.1)$$

The second term here is a time derivative, which vanishes for static fields. The third and fourth terms are of the form $(\tilde{\Gamma})^2$, and since $\tilde{\Gamma}$ is first-order in the metric perturbation, these contribute only at second order and can be neglected, giving

$$\tilde{R}_{00} = \tilde{R}_{0A0}^A = \partial_A \left(\frac{1}{2} \tilde{g}^{AC} (\partial_0 \tilde{g}_{C0} + \partial_0 \tilde{g}_{0C} - \partial_C \tilde{g}_{00}) \right) = -\frac{1}{2} \tilde{g}^{AB} \partial_A \partial_B \tilde{\gamma}_{00}. \quad (2.2)$$

For the static solution, the time derivative also vanishes, and the equation becomes

$$\partial_\zeta^2 \tilde{\gamma}_{00} + \partial_x^2 \tilde{\gamma}_{00} + \partial_y^2 \tilde{\gamma}_{00} + \partial_z^2 \tilde{\gamma}_{00} = 0. \quad (2.3)$$

Here ζ is the fifth dimension, which we also sometimes refer to as the background dimension. It is somehow related to the matter distribution in the entire universe and is responsible for the inertial properties of matter [38]. Under the assumption of spherical symmetry of the special part, it can be written as

$$\partial_\zeta^2 (r \tilde{\gamma}_{00}) + \partial_r^2 (r \tilde{\gamma}_{00}) = 0. \quad (2.4)$$

Using ‘separation of variables’ and considering $(r \tilde{\gamma}_{00}) = R(r)\chi(\zeta)$, we get

$$\frac{1}{R} \frac{\partial^2 R}{\partial r^2} = -\frac{1}{\chi} \frac{\partial^2 \chi}{\partial \zeta^2} = \lambda^2, \quad (2.5)$$

where, λ is a constant. This gives

$$R = P_1 e^{\lambda r} + P_2 e^{-\lambda r}, \quad \chi = Q_1 \cos(\lambda \zeta) + Q_2 \sin(\lambda \zeta), \quad (2.6)$$

where, P_1, P_2, Q_1 and Q_2 are constants. The term $\tilde{\gamma}_{00}$, under weak-field approximation is a first-order perturbation, and it cannot increase exponentially with distance. Therefore, taking $P_1 = 0$, we can get

$$(r \tilde{\gamma}_{00}) = S + P_2 e^{-\lambda r} (Q_1 \cos(\lambda \zeta) + Q_2 \sin(\lambda \zeta)). \quad (2.7)$$

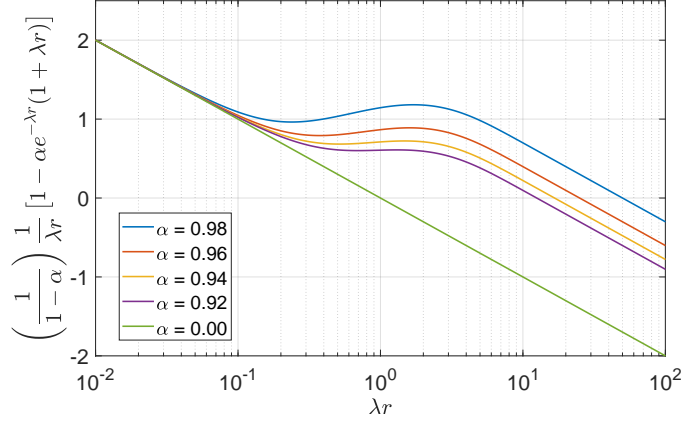


Figure 1. For different α there is a range of λr for which the curve simply flattens out.

S is constant, coming from the complimentary function of the differential equation. If we consider that over a place (a scale of the order of a galaxy) the background is almost similar then the change in ζ is really small. Therefore, here we may just take $\lambda\zeta \sim 0$. There is a constant factor of \hbar multiplied which is also very small. So, in this limit $\cos(\lambda\zeta) \rightarrow 1$ and $\sin(\lambda\zeta) \rightarrow 0$.

Relating it with Newtonian gravity, we get $\tilde{\gamma}_{00} = 2\Phi$, where Φ is the Newtonian potential of the gravitational field. Replacing these limiting values in Eq.(2.7) and substituting $P_2Q_1 = 2KM$ and $S = 2(1 + K)M$ and replacing $\tilde{\gamma}_{00} = 2\Phi$ we can get the potential as

$$\Phi = \frac{GM}{r} [1 + K(1 - e^{-\lambda r})]. \quad (2.8)$$

Here, M is the mass at the center and G is the Newton's gravitational constant. λ and K are the background-dependent quantities. They may depend on mass M but are independent on r . Observations of galactic velocity profiles indicate that λ^{-1} typically falls within the order of a few kpc. For small values of r , the exponential term $e^{-\lambda r}$ approaches unity. Consequently, the potential Φ assumes the shape of the Newtonian potential, given by $\Phi = \frac{GM}{r}$.

This alignment with the Newtonian potential is particularly significant on the scale of the solar system. In the asymptotic limit of $r \rightarrow \infty$, the exponential term goes to 0. Hence, for large values of r , it becomes $(1 + K)$ times that of Newtonian potential and can provide additional gravitational force in large gravitationally balanced systems, such as galaxies, galaxy clusters, etc. A similar form of potential has previously been used by other groups to explain the galactic velocity profile correctly [24–27, 44].

It is important to emphasize that both K and λ should remain independent of the mass of the gravitating objects, as any such dependence would lead to a violation of symmetry. To illustrate this point, consider a scenario where two particles mutually exert gravitational attraction on each other. If K were to rely on the mass of just one of these particles, the equation governing gravitational energy would become asymmetric with respect to the masses of both particles. Consequently, in order to preserve symmetry, K and λ are not influenced by the masses of the interacting entities. Instead, K and λ are shaped by the combined mass distribution of all other particles that exist nearby. Specifically, if there were only two particles in the universe, then K should be 0. However, upon introducing a third particle, its presence alters the gravitational interaction between the initial two particles through the K and λ term.

This also aligns with the fundamental concepts of Mach's principle, which proposes that local physical phenomena are interconnected with the distribution of matter throughout the universe. In essence, the influence of neighboring masses is coming into the gravitational energy through the K and λ .

As the potential due to a static spherically symmetric gravitational field is given by Eq.(2.8), we can calculate the acceleration due to the gravitational field as $\frac{\partial\Phi}{\partial r}$. If a particle is orbits mass M

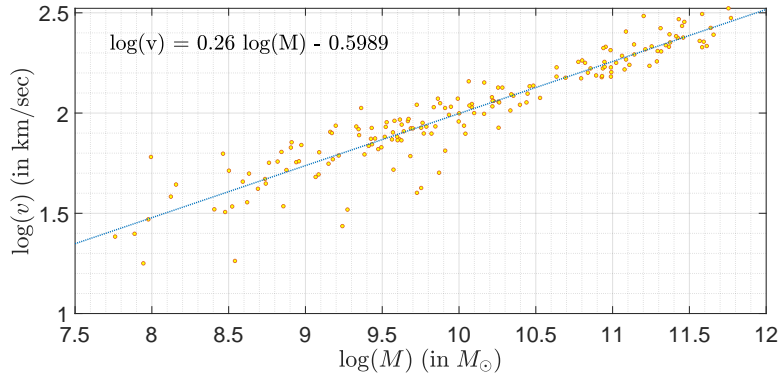


Figure 2. The graph illustrates the measured velocities at the outer edges of 175 SPARC galaxies against the masses of these galaxies. Additionally, a blue straight line represents the optimal fit through these data points, accompanied by the equation characterizing this linear fit. The graph provides $M \sim v^{3.85}$, aligning with the expectations of the Tully Fisher relation.

in a circular orbit of radius r , and its orbital velocity is v , then we can calculate v by equating the centripetal force with the gravitational field, giving

$$v^2 = \frac{GM}{r} [1 + K(1 - e^{-\lambda r}(1 + \lambda r))] = \frac{GM(1 + K)\lambda}{\lambda r} [1 - \alpha e^{-\lambda r}(1 + \lambda r)]. \quad (2.9)$$

where $\alpha = \frac{K}{1+K}$. The velocity has some interesting property. For $\alpha \in (0.92, 0.95)$ and $\lambda r \in (0.4, 2.5)$ the velocity becomes almost independent of r . This can be seen in Fig. 3. From the range of α we can derive the range of K to be $\in (11, 19)$.

The velocity in the outer part of the spiral galaxies (rotationally bounded system) does not decrease with increasing radius, as suggested by Keplerian velocity. In fact, it is almost independent of radius r . Therefore, Eq. 2.9 can be used to explain the velocity profile of spiral galaxies. This was first explained in [45, 46].

For this particular range of r , the velocity of the test particle behaves as $v^2 \sim GM(1 + K)\lambda$. However, according to the Tully–Fisher relation, the mass of a spiral galaxy is linked to its asymptotic velocity as $M \sim v^\gamma$, where $\gamma \in (3.5, 4)$. If we assume that $M \sim v^4$, then we can take

$$(1 + K) \propto \frac{1}{\sqrt{M}} \quad \implies \quad K = \sqrt{\frac{M_c}{M}} - 1 \quad (2.10)$$

Here M_c is some constant mass. Putting everything together, the expression for the final velocity becomes

$$v^2 = \frac{GM}{r} \left[1 + \left(\sqrt{\frac{M_c}{M}} - 1 \right) (1 - e^{-\lambda r}(1 + \lambda r)) \right]. \quad (2.11)$$

This equation follows Newtonian velocity for a particle in orbit for $\lambda r \ll 1$. For $\lambda r \in (0.4, 2.5)$, velocity becomes constant and follows the Tully Fisher relation i.e., $v^4 \sim M$. Finally for $\lambda r \gg 2.5$, it behaves as $v^2 \sim \frac{\sqrt{M}}{r}$. At this point, we should also like to point out that K is a background-dependent quantity. For spiral galaxy K follows relation Eq. 2.10 does not imply that K should follow similar expressions for any kind of mass distribution. For other kinds of mass distribution, the form of K may vary.

3 A brief overview of SPARC galaxy database

An ideal galaxy sample should include all the galaxies within a sufficiently extensive volume of the universe [47]. However, in practice, such a sample can never exist as there will be limitations on the

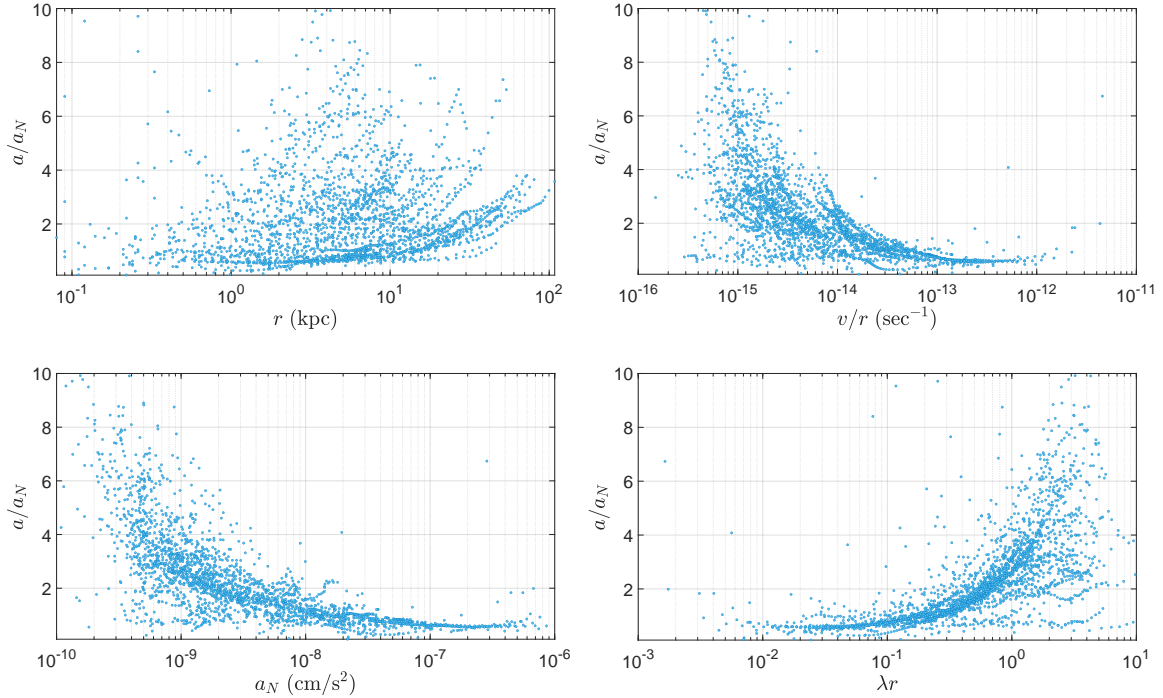


Figure 3. The figure illustrates the relationship between mass discrepancy to four variables: r , v/r , a_N , and λr . These plots are based on a dataset comprising 2385 data points from the SPARC galaxies. None of the plots exhibit a very prominent correlation. Specifically, the top two plots display relatively weaker correlations and appear more dispersed, whereas the bottom two plots show relatively stronger correlations.

minimum luminosity and surface brightness of galaxies below which the galaxies can not be detected. Therefore, the best thing is to sample randomly across the mass function [48].

SPARC (Spitzer Photometry and Accurate Rotation Curves) database provides a sample of 175 nearby galaxies with new surface photometry at $3.6\mu\text{m}$ and high-quality rotation curves from previous HI/H α studies [49]. SPARC rotation curves are drawn from multiple papers. The rotation curves are generally smooth but can show large-scale features with a direct correspondence in the surface brightness profile, in agreement with Renzo’s rule: “For any feature in the luminosity profile, there is a corresponding feature in the rotation curve and vice versa” [50, 51].

The baryonic velocity is divided into three components, the gas velocity v_{gas} , disk velocity v_{disc} , and the bulge velocity v_{bul} . The total baryonic velocity is defined as

$$v_{bar} = \sqrt{\epsilon_{gas}v_{gas}^2 + \epsilon_{disc}\gamma_{disc}v_{disc}^2 + \epsilon_{bul}\gamma_{bul}v_{bul}^2}. \quad (3.1)$$

γ_{disc} and γ_{bul} are the mass to light ratio of the stars in the disc and the bulge. $\epsilon_{...}$ represents the signature of different components of the velocities, which in some cases can be negative. Most importantly V_{gas} can sometimes be negative in the innermost regions: this occurs when the gas distribution has a significant central depression and the material in the outer regions exerts a stronger gravitational force than that in the inner parts [49].

The values of v_{disc} and v_{bul} are provided for $\gamma_{disc}, \gamma_{bul} = 1$. Ideally $v_{obs} > v_{bar}$. However, in the SPARC dataset there are some galaxies for which $v_{bar}/v_{obs} > 1$, mostly at the low radius. There are many such galaxies however, the issue is severe for about 21 galaxies. This may be due to the fixed γ value as described by [49].

For our calculations, we have used v_{bar} given in the SPARC data set and then we obtain $M(r)$ inside a radius r using $M(r) = v_{bar}^2 r / G$. In Fig. 2, we have plotted the velocity at the outermost data point of all 175 galaxies against mass of the galaxies. The best linear fit is given by

$$\log(v) = 0.26 \log(M) - 0.5989. \quad (3.2)$$

This is equivalent to $M \sim v^{3.85}$, which is in agreement with the Tully-Fisher relation [52].

4 Testing the theory against observations

The core objective of this article is to investigate whether Machian gravity can offer an explanation for observed galactic phenomena. We use Eq. 2.11 to fit it with 175 SPARC galaxies. The primary parameters in our analysis are M_c and λ^{-1} , which are determined for each of the galaxies using MCMC analysis. The results have been shown in Table 1.

Fig. 3 displays the mass discrepancy of the galaxies against various parameters. This discrepancy is quantified through the ratio of observed acceleration to the Newtonian acceleration, computed from the luminous mass of the galaxy. Mathematically, this can be expressed as [53]:

$$\frac{a}{a_N} = \frac{v_{obs}^2}{v_{bar}^2}. \quad (4.1)$$

In our investigation, we exclude 21 galaxies with $v_{bar}/v_{obs} > 1$, as these are likely a consequence of fixed mass-to-light ratio selections, as discussed in [49]. Among the remaining 154 galaxies, several data points exhibit $v_{bar}/v_{obs} > 1$ at smaller radii, although the errors may not be severe. Overall, we plot a total of 2385 data points.

Different galaxies have distinct rotation curves. Given the substantial dataset encompassing numerous galaxies, it is expected that the resulting plot would exhibit a scattered pattern. This is indeed evident in the first plot (top-left) of Fig. 3, which illustrates mass discrepancies in relation to radius. We can see that there are galaxies where the mass discrepancy is not apparent at low radii while there are other galaxies where the mass discrepancy kicks in even at a very small radius. The lack of a fixed radius where mass discrepancy consistently occurs differs from what one might anticipate if a purely baryon-independent cold dark matter governed the galaxy's dynamics.

A similar scenario emerges in the subsequent plot (top-right), illustrating mass discrepancy against orbital angular velocity. The plot shows a slightly higher correlation with the mass discrepancy. However, the scatter plot highlights the absence of a high correlation between the two. In contrast, the lower-left plot depicting mass discrepancy against Newtonian acceleration reveals a noticeable correlation. Generally, the mass deficiency becomes apparent beyond an acceleration of $a = 10^{-8} \text{ cm/s}^2$. Consequently, it establishes a connection between the Newtonian acceleration and mass deficiency. Various authors have explored this linkage in previous works, including [53–55].

The last (bottom-right) plot depicts the mass deficiency against λr , where the best-fit λ value has been individually computed for each galaxy. Once again, a robust correlation emerges between mass discrepancy and λr . Mass discrepancy becomes apparent for $\lambda r > 0.3$, and this pattern of discrepancy is prevalent in nearly all galaxies within the range of $\lambda r \in (0.3, 5)$. This range aligns with our earlier expectations from the preceding section. This observation bears significant implications, particularly concerning theories such as MoG and TeVeS, which introduce additional massive scalar and vector fields. However, the fixed mass of these fields renders them unable to account for this observed relationship.

These trends can be explained through mathematical analysis. Referring to Eq. 2.11, it is evident that the equation gives a radius-independent velocity as $\lambda r \rightarrow 1$. Therefore, expanding the velocity in a Taylor series centered around $\lambda r \rightarrow 1$ we can get:

$$\begin{aligned}
v^2 &= \frac{GM}{r} \left[1 + \left(\sqrt{\frac{M_c}{M}} - 1 \right) (1 - e^{-1} (3 - \lambda r)) \right] \\
&= \frac{GM}{r} \left[3e^{-1} + \left(\sqrt{\frac{M_c}{M}} \lambda r e^{-1} - \lambda r e^{-1} \right) + (1 - 3e^{-1}) \sqrt{\frac{M_c}{M}} \right] \\
\frac{v^2}{r} &\approx \frac{GM}{r^2} \left[1.1 + 0.37 \sqrt{\frac{GM_c}{\lambda^{-2} GM}} - 0.37 \lambda r - 0.1 \sqrt{\frac{M_c}{M}} \right] \tag{4.2}
\end{aligned}$$

Now provided $\lambda r > 0.27$ the second term will dominate over the 4th term. Also, if we assume that $\frac{M_c}{M} \sim 10 - 50$, then the third term is also small. Therefore, if we ignore these terms, we can write the equation as

$$a \approx a_N \left[0.73 + 0.37 \sqrt{\frac{a_0}{a_N}} \right] = a_N \mu \left(\frac{a_0}{a_N} \right). \tag{4.3}$$

Here, $a_N = \frac{GM}{r^2}$ is the Newtonian acceleration, while $a_0 = \frac{GM_c}{\lambda^{-2}}$ is a characteristic acceleration. μ is a function. Consequently, near the galaxy's periphery or when $\lambda r \rightarrow 1$, our equation behaves as MOND. Therefore, the mass discrepancy is predominantly linked to acceleration, with a slight dependence on λr . This $\lambda r \rightarrow 1$ dependence is consistent with the findings in Fig. 3. As the mass discrepancy is influenced by $a_0 = \frac{GM_c}{\lambda^{-2}}$, it also shows that M_c and λ are not entirely independent. Instead, we should expect a strong correlation between M_c and λ^{-2} .

In Fig. 4, we present the distributions derived from our MCMC analysis for two randomly selected galaxies, NGC0247 and UGC12732. The first two plots in the upper row show the distributions for λ^{-1} and M_c , respectively, while the third plot depicts their correlation. Evidently, a robust correlation emerges between λ^{-2} and M_c , showing the influence of $a_0 = \frac{GM_c}{\lambda^{-2}}$ on gravitational field.

The second row displays the χ^2 distribution against λ^{-1} , M_c , and a_0 respectively. Strikingly, the χ^2 distributions consistently exhibit a single minimum across all these parameters. This observation bears significance. If the gravitational equation were governed by MOND-like formulations where the gravitational force exclusively depends on a characteristic a_0 , we would not get such singular minima in the χ^2 plots when plotted against λ^{-1} or M_c . This is because if a_0 constituted the sole parameter of the theory, there would be an infinite number of possible combinations of λ and M_c resulting in the same a_0 value. While we show only two galaxies, the analysis is carried out on all 175 galaxies. Remarkably, apart from a few exceptions, all galaxies exhibited a singular minimum χ^2 value, further reinforcing the consistency of the findings.

To sum up, in Fig. 5, we have shown the rotational curves of the 154 SPARC galaxies. The red dots with green errorbars represent the observed velocities from the SPARC dataset. The blue dotted line shows the expected velocity profile from the baryonic matter calculated using standard Newtonian mechanics. The red line represents Machian Gravity fit to the velocity profile.

It is interesting to see that many galaxies have unique velocity profiles. Importantly, each feature within the observed velocity profiles corresponds to a corresponding feature in the velocity profiles calculated from the baryonic matter using Newtonian dynamics. Such correspondence poses a challenge for explanations invoking dark matter, which lacks strong coupling to baryonic matter. Intriguingly, the Machian Gravity model is remarkably effective in explaining the velocity profiles, entirely avoiding the need for dark matter.

Fig. 6 depicts the rotational profile for the remaining 21 galaxies. A visual inspection of these plots suggests potential issues with the mass model for these galaxies. In these cases, the velocity derived from the baryonic mass using Newtonian mechanics significantly exceeds the observed velocities, hinting at potential inconsistencies between the model and the data.

Table 1 provides a summary of our findings, showcasing the best-fit values for M_c , λ^{-1} , and a_0 across various galaxies. These values are accompanied by other galaxy-specific details like baryonic mass and radius. Notably, we observe that while λ^{-1} varies significantly from galaxy to galaxy, for

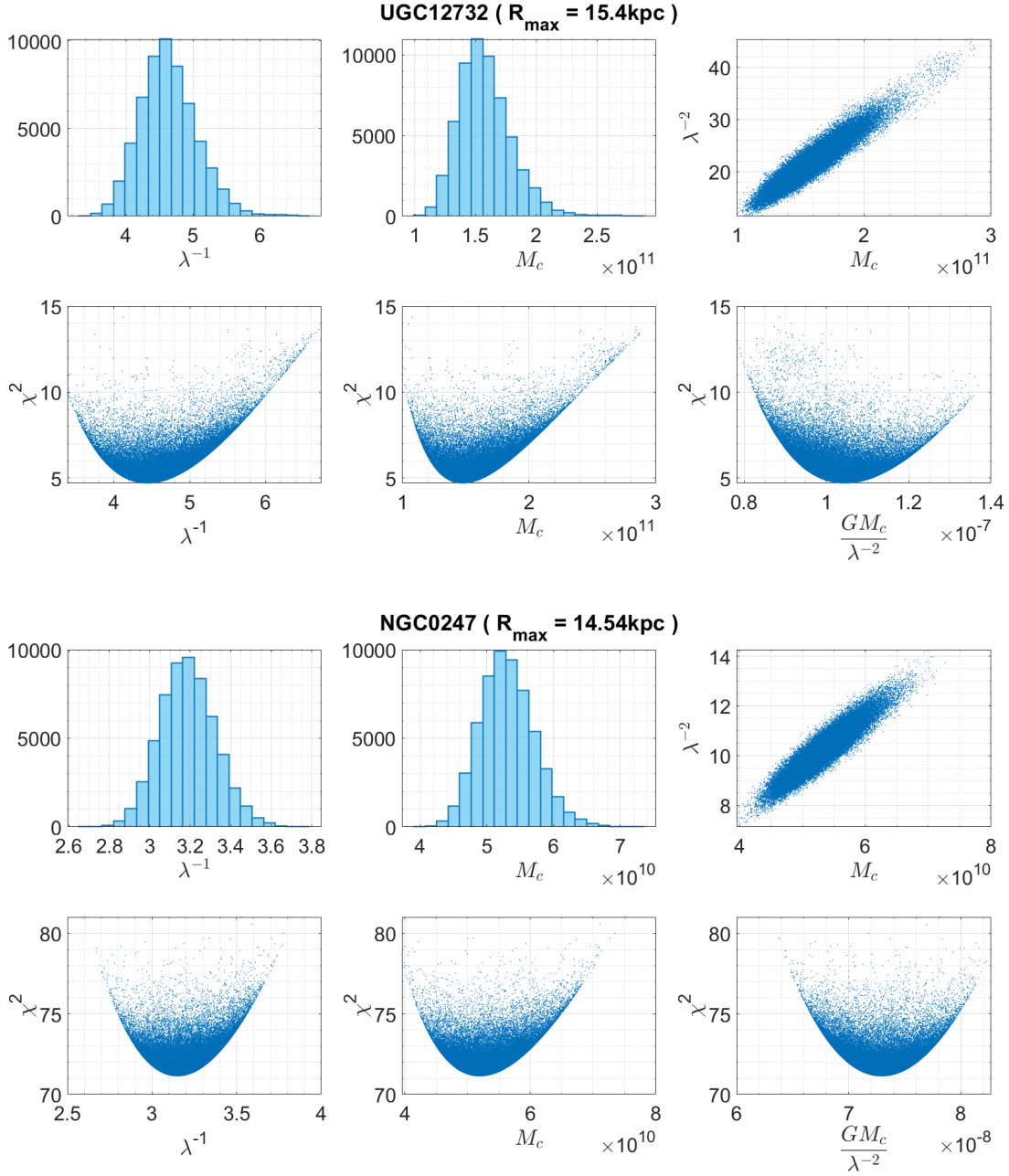


Figure 4. The illustration portrays the distributions of λ^{-1} and M_c , their correlation, and the relationship of χ^2 with these parameters, alongside $a_0 = \frac{GM_c}{\lambda^{-2}}$. In the figure, λ^{-1} is scaled in kiloparsecs (kpc) and M_c is scaled in solar masses (M_\odot). Notably, the value of a_0 for the best-fit χ^2 is approximately on the order of 10^{-8} cm/s^2 . The value of R_{max} corresponds to the radius of the last velocity data point for each galaxy. Importantly, λ^{-1} aligns roughly with the order of R_{max} .

147 out of 175 galaxies, $\lambda^{-1}r$ falls within the range of (0.1, 5) for all galaxies. This suggests that using a fixed value of λ as often done might not fully capture the complexity of all velocity profiles [25, 56].

Moreover, we notice a considerable variation in the acceleration parameter a_0 among different galaxies. Even though these values might roughly be on the order of 10^{-8} cm/s^2 , the extent of this

variation indicates that a single acceleration value may not be sufficient to comprehensively explain all galaxies, which contrasts with claims made by MOND theories.

5 Discussion and Conclusion

This study shows how the Machian gravity (MG) model, as proposed in [38–40, 57], can explain spiral galactic velocity profiles using the SPARC database. Spiral galaxies, being rotationally bound systems, require dark matter to account for their velocity profiles. Over time, various modified gravity theories have been put forth to explain these velocity profiles in spiral galaxies empirically. Our investigation demonstrates how Machian gravity aligns with these empirical formulations.

The velocity profile for spiral galaxies in MG is characterized by Eq. 2.11. It has two parameters: a characteristic mass scale M_c and a length scale λ^{-1} . Our analysis reveals that the length scale λ^{-1} is comparable with the radius of the galaxy and varies across different galaxies. Consequently, the conventional approach of adopting a fixed λ , as postulated by some prior researchers [25], may not comprehensively capture the intricacies of galactic velocity profiles.

Furthermore, we establish that near the edge of a galaxy, where $\lambda r \rightarrow 1$, an acceleration scale emerges, $a_0 = \frac{GM_c}{\lambda^{-2}}$. In this region, the stellar acceleration tends to a MOND-like behavior dictated by this acceleration scale. However, our analysis also shows that this acceleration scale diverges for different galaxies, depending on their individual structures. Although these accelerations approximately measure around 10^{-8}cm/sec^2 , their variability across galaxies suggests that a single acceleration scale might not completely account for the entire dataset. Our findings also reveal that beyond acceleration, a galaxy’s mass discrepancy also hinges on λr , a factor not previously explored in existing research.

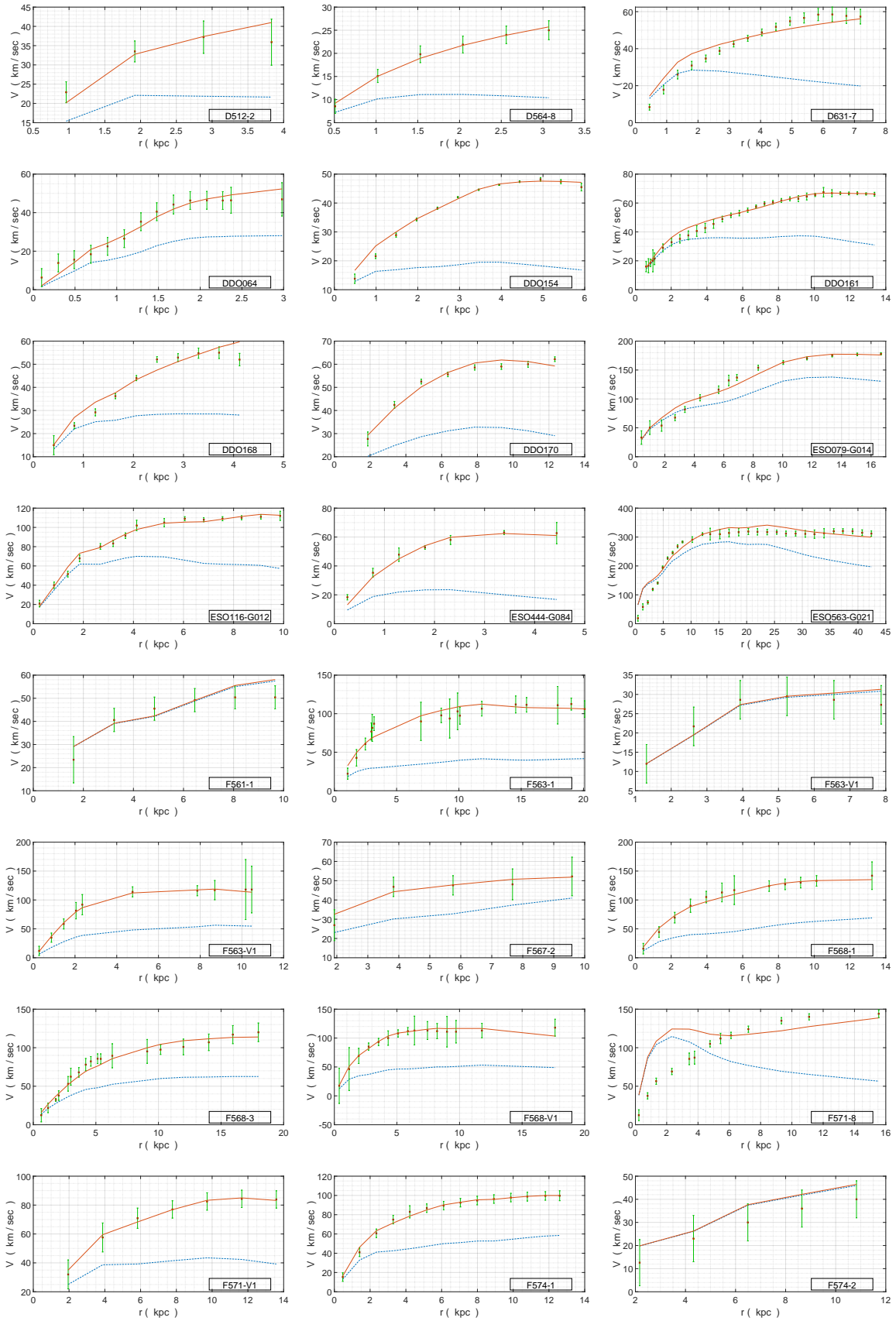
Importantly, while several other modified gravity has been designed to explain observational phenomena, the Machian gravity model stands apart from these theories as it emerges from a purely mathematical quest to formulate Mach’s principle. Notably, this model adeptly explains the galactic velocity profiles of 154 SPARC galaxies, demonstrating remarkable agreement. For the remaining 21 galaxies, discrepancies in the mass model are apparent, suggesting potential inaccuracies. We are confident that refining the mass model for these galaxies through parameter adjustments, such as varying the mass-to-light ratio, could potentially align their velocities with the predictions of the Machian gravity model.

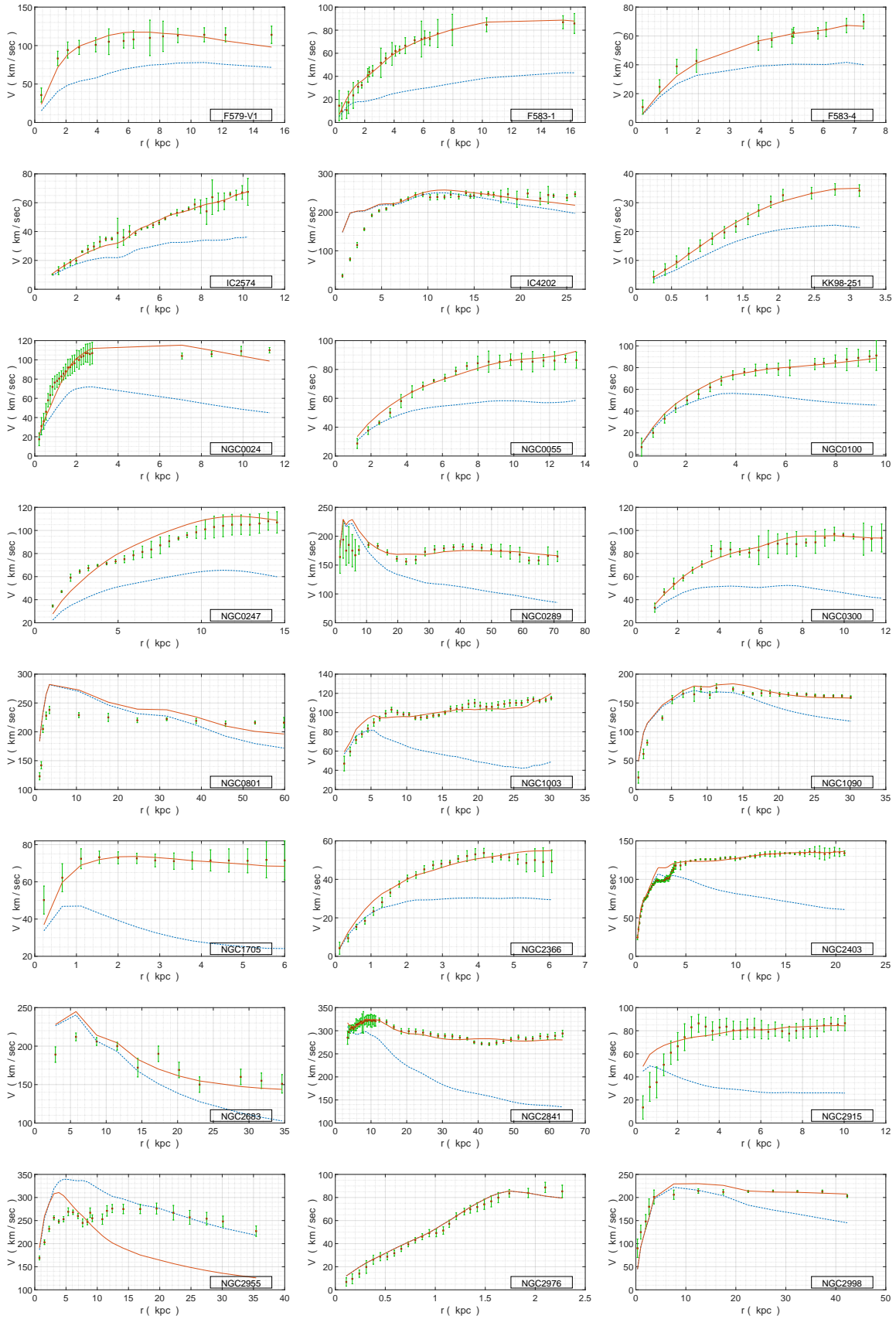
References

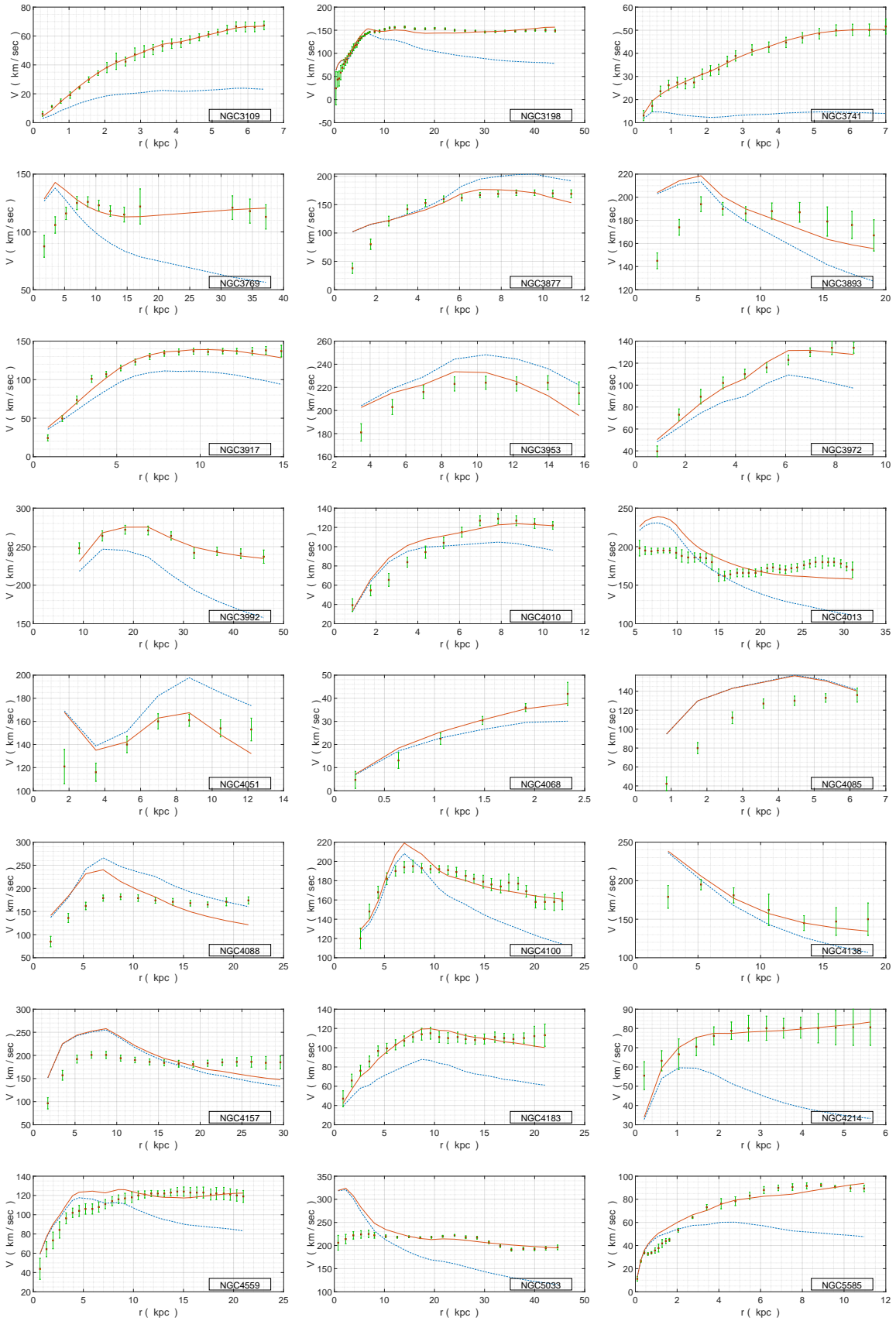
- [1] V.C. Rubin, W.K. Ford Jr and N. Thonnard, *Rotational properties of 21 sc galaxies with a large range of luminosities and radii, from ngc 4605/r= 4kpc/to ugc 2885/r= 122 kpc*, *Astrophysical Journal, Part 1, vol. 238, June 1, 1980*, p. 471-487. **238** (1980) 471.
- [2] M. Persic, P. Salucci and F. Stel, *The universal rotation curve of spiral galaxies—i. the dark matter connection*, *Monthly Notices of the Royal Astronomical Society* **281** (1996) 27.
- [3] A. Borriello and P. Salucci, *Dark halos around spirals; no role for collisionless cold dark matter particles*, Tech. Rep. (2001).
- [4] J. Binney and S. Tremaine, *Galactic dynamics*, vol. 20, Princeton university press (2011).
- [5] S.P. Martin, *A SUPERSYMMETRY PRIMER*, in *Perspectives on Supersymmetry*, pp. 1–98, WORLD SCIENTIFIC (1998), DOI.
- [6] E.W. Mielke and F.E. Schunck, *Nontopological scalar soliton as dark matter halo*, *Physical Review D* **66** (2002) 023503.
- [7] J. Mbelek, *Modelling the rotational curves of spiral galaxies with a scalar field*, *Astronomy & Astrophysics* **424** (2004) 761.
- [8] X. Hernández, T. Matos, R.A. Sussman and Y. Verbin, *Scalar field “mini-machos”: A new explanation for galactic dark matter*, *Physical Review D* **70** (2004) 043537.
- [9] C. Boehmer and T. Harko, *Can dark matter be a bose–einstein condensate?*, *Journal of Cosmology and Astroparticle Physics* **2007** (2007) 025.

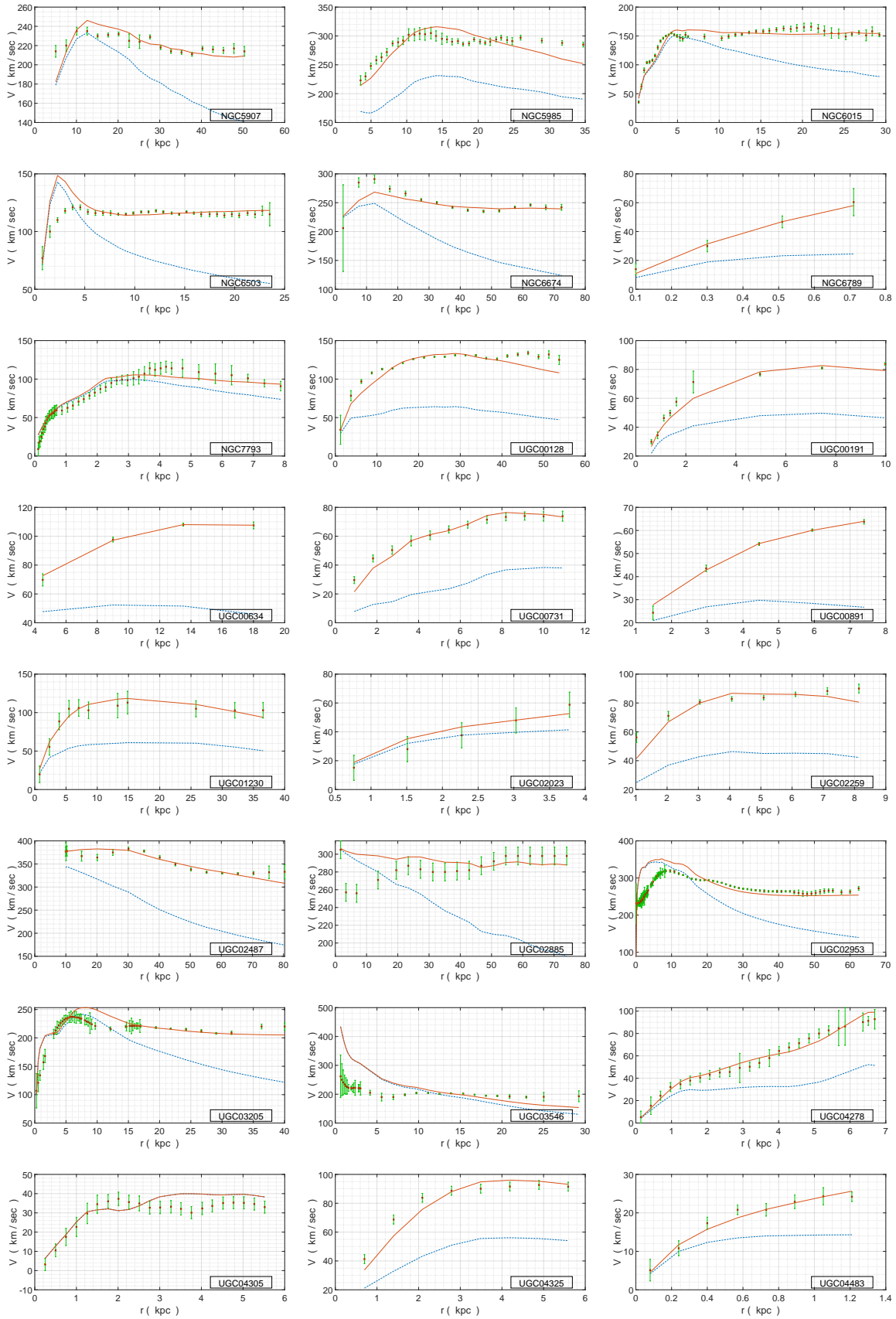
- [10] D. Bertacca, N. Bartolo and S. Matarrese, *Halos of unified dark matter scalar field*, *Journal of Cosmology and Astroparticle Physics* **2008** (2008) 005.
- [11] J.-W. Lee, *Are galaxies extending?*, *Physics Letters B* **681** (2009) 118.
- [12] J.L. Cervantes-Cota, M.A. Rodriguez-Meza, D. Nunez et al., *Spherical scalar-tensor galaxy model*, *Physical Review D* **79** (2009) 064011.
- [13] J.-W. Lee and S. Lim, *Minimum mass of galaxies from bec or scalar field dark matter*, *Journal of Cosmology and Astroparticle Physics* **2010** (2010) 007.
- [14] T. Harko, *Galactic rotation curves in modified gravity with nonminimal coupling between matter and geometry*, *Physical Review D* **81** (2010) 084050.
- [15] F. Wilczek, *Problem of strong p and t invariance in the presence of instantons*, *Phys. Rev. Lett.* **40** (1978) 279.
- [16] J.-w. Lee and I.-g. Koh, *Galactic halos as boson stars*, *Phys. Rev. D* **53** (1996) 2236.
- [17] M. Milgrom, *A Modification of the Newtonian dynamics as a possible alternative to the hidden mass hypothesis*, *Astrophys.J.* **270** (1983) 365.
- [18] M. Milgrom, *A Modification of the Newtonian dynamics: Implications for galaxies*, *Astrophys.J.* **270** (1983) 371.
- [19] M. Milgrom, *A modification of the Newtonian dynamics: implications for galaxy systems*, *Astrophys.J.* **270** (1983) 384.
- [20] M. Milgrom, *MD or DM? Modified dynamics at low accelerations vs dark matter*, *PoS HRMS2010* (2010) 033 [[1101.5122](#)].
- [21] J. Bekenstein and M. Milgrom, *Does the missing mass problem signal the breakdown of Newtonian gravity?*, *Astrophys.J.* **286** (1984) 7.
- [22] J.D. Bekenstein, *Relativistic MOND as an alternative to the dark matter paradigm*, *Nucl.Phys.* **A827** (2009) 555C [[0901.1524](#)].
- [23] M. Milgrom, *Solutions for the modified Newtonian dynamics field equation*, *Astrophys.J.* **302** (1986) 617.
- [24] J. Moffat, *Scalar-tensor-vector gravity theory*, *JCAP* **0603** (2006) 004 [[gr-qc/0506021](#)].
- [25] J. Brownstein and J. Moffat, *Galaxy rotation curves without non-baryonic dark matter*, *Astrophys.J.* **636** (2006) 721 [[astro-ph/0506370](#)].
- [26] J. Brownstein and J. Moffat, *Galaxy cluster masses without non-baryonic dark matter*, *Mon.Not.Roy.Astron.Soc.* **367** (2006) 527 [[astro-ph/0507222](#)].
- [27] J. Moffat and V. Toth, *Modified Gravity: Cosmology without dark matter or Einstein's cosmological constant*, [0710.0364](#).
- [28] J.D. Bekenstein, *Relativistic gravitation theory for the MOND paradigm*, *Phys.Rev.* **D70** (2004) 083509 [[astro-ph/0403694](#)].
- [29] H. van Dam and M. Veltman, *Massive and massless Yang-Mills and gravitational fields*, *Nucl.Phys.* **B22** (1970) 397.
- [30] V. Zakharov, *Linearized gravitation theory and the graviton mass*, *JETP Lett.* **12** (1970) 312.
- [31] E. Babichev, C. Deffayet and R. Ziour, *The Recovery of General Relativity in massive gravity via the Vainshtein mechanism*, *Phys.Rev.* **D82** (2010) 104008 [[1007.4506](#)].
- [32] E. Babichev and M. Crisostomi, *Restoring general relativity in massive bigravity theory*, *Phys.Rev.* **D88** (2013) 084002 [[1307.3640](#)].
- [33] J. Overduin and P. Wesson, *Kaluza-Klein gravity*, *Phys.Rept.* **283** (1997) 303 [[gr-qc/9805018](#)].
- [34] J. Ponce de Leon and P.S. Wesson, *Exact solutions and the effective equation of state in Kaluza-Klein theory*, *Journal of Mathematical Physics* **34** (1993) 4080.
- [35] P.S. Wesson and J.P. de Leon, *Kaluza-Klein equations, Einstein's equations, and an effective energy-momentum tensor.*, *Journal of Mathematical Physics* **33** (1992) 3883.

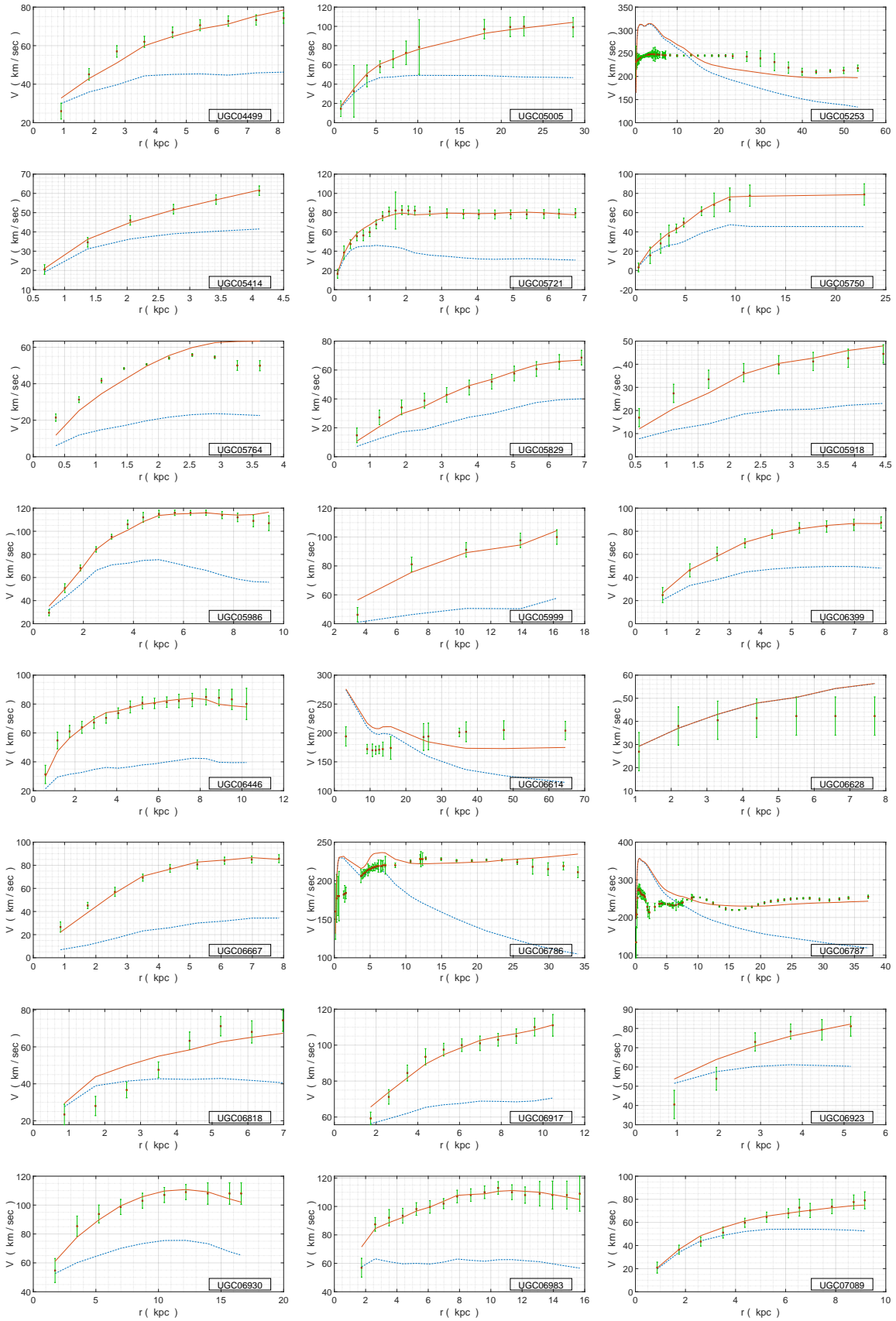
- [36] J.P. de Leon, *Schwarzschild-like exteriors for stars in kaluza-klein gravity*, *arXiv preprint arXiv:1003.3151* (2010) .
- [37] P. Moraes, *Cosmic acceleration from varying masses in five dimensions*, *International Journal of Modern Physics D* **25** (2016) 1650009.
- [38] S. Das, *Aspects of machian gravity (i): A mathematical formulation for mach's principle*, 2023.
- [39] S. Das, *Mach's principle and the origin of the quantum phenomenon*, [1206.0923](#).
- [40] S. Das, *Machian gravity and a cosmology without dark matter and dark energy*, 2015.
- [41] D.W. Sciama, *On the origin of inertia*, *Monthly Notices of the Royal Astronomical Society* **113** (1953) 34.
- [42] M.S. Berman, *On the machian origin of inertia*, *Astrophysics and Space Science* **318** (2008) 269.
- [43] D.W. Sciama, *The physical structure of general relativity*, *Reviews of Modern Physics* **36** (1964) 463.
- [44] J. Moffat and V. Toth, *Fundamental parameter-free solutions in modified gravity*, *Class.Quant.Grav.* **26** (2009) 085002 [[0712.1796](#)].
- [45] R. Sanders, *Anti-gravity and galaxy rotation curves*, *Astronomy and Astrophysics (ISSN 0004-6361)*, vol. 136, no. 2, July 1984, p. L21-L23. **136** (1984) L21.
- [46] R.H. Sanders and S.S. McGaugh, *Modified newtonian dynamics as an alternative to dark matter*, *Annual Review of Astronomy and Astrophysics* **40** (2002) 263.
- [47] K.D. Eckert, S.J. Kannappan, D.V. Stark, A.J. Moffett, M.A. Norris, E.M. Snyder et al., *Resolve survey photometry and volume-limited calibration of the photometric gas fractions technique*, *The Astrophysical Journal* **810** (2015) 166.
- [48] S. McGaugh, F. Lelli, P. Li and J. Schombert, *Dynamical regularities in rotating galaxies*, *Proceedings of the International Astronomical Union* **14** (2019) 144.
- [49] F. Lelli, S.S. McGaugh and J.M. Schombert, *SpArc: Mass models for 175 disk galaxies with spitzer photometry and accurate rotation curves*, *The Astronomical Journal* **152** (2016) 157.
- [50] R. Sancisi, *The visible matter - dark matter coupling*, 2003.
- [51] M.H. Chan, *Two mysterious universal dark matter-baryon relations in galaxies and galaxy clusters*, 2022.
- [52] R.B. Tully and J.R. Fisher, *A new method of determining distances to galaxies*, *Astronomy and Astrophysics*, vol. 54, no. 3, Feb. 1977, p. 661-673. **54** (1977) 661.
- [53] S.S. McGaugh, *The mass discrepancy-acceleration relation: disk mass and the dark matter distribution*, *The Astrophysical Journal* **609** (2004) 652.
- [54] M. Milgrom, *Mond—a pedagogical review*, 2001.
- [55] I. Banik and H. Zhao, *From galactic bars to the hubble tension: Weighing up the astrophysical evidence for milgromian gravity*, *Symmetry* **14** (2022) 1331.
- [56] M. Green and J. Moffat, *Modified gravity (MOG) fits to observed radial acceleration of SPARC galaxies*, *Physics of the Dark Universe* **25** (2019) 100323.
- [57] S. Das, *Aspects of Machian gravity III: Understanding the galaxy clusters*, .

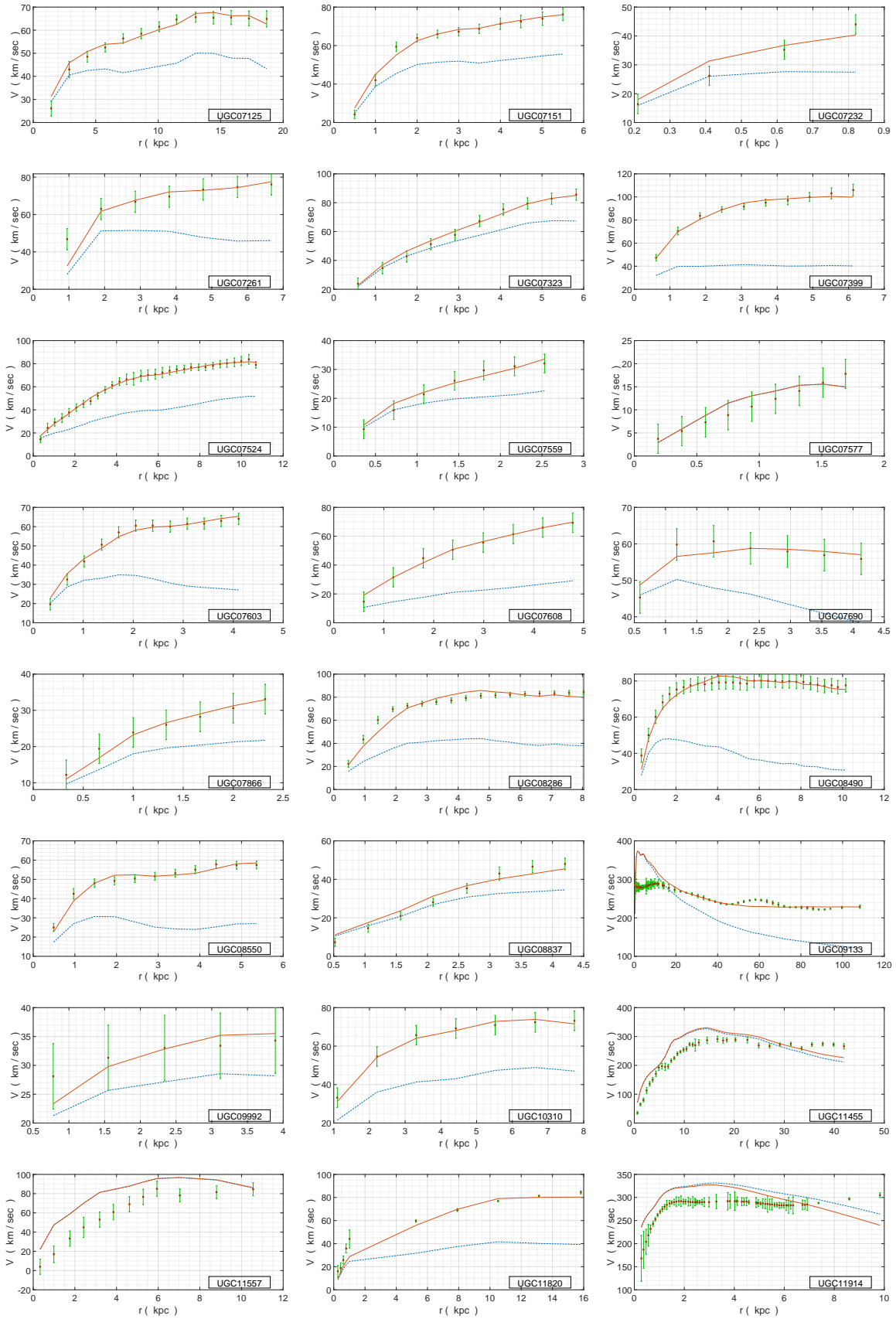












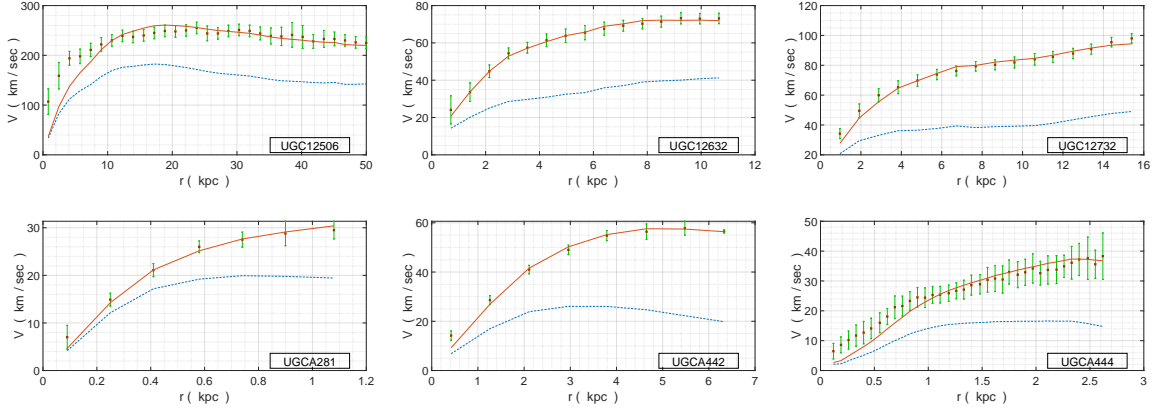


Figure 5. The illustration depicts the Machian Gravity (MG) fitting applied to the SPARC galaxy dataset. The red dots, accompanied by green error bars show the observed velocities of the SPARC dataset. The blue dotted curve represents the velocity computed using Newtonian Mechanics based on the baryonic matter, while the solid red curve reflects the velocity computed employing the Machian gravity model.

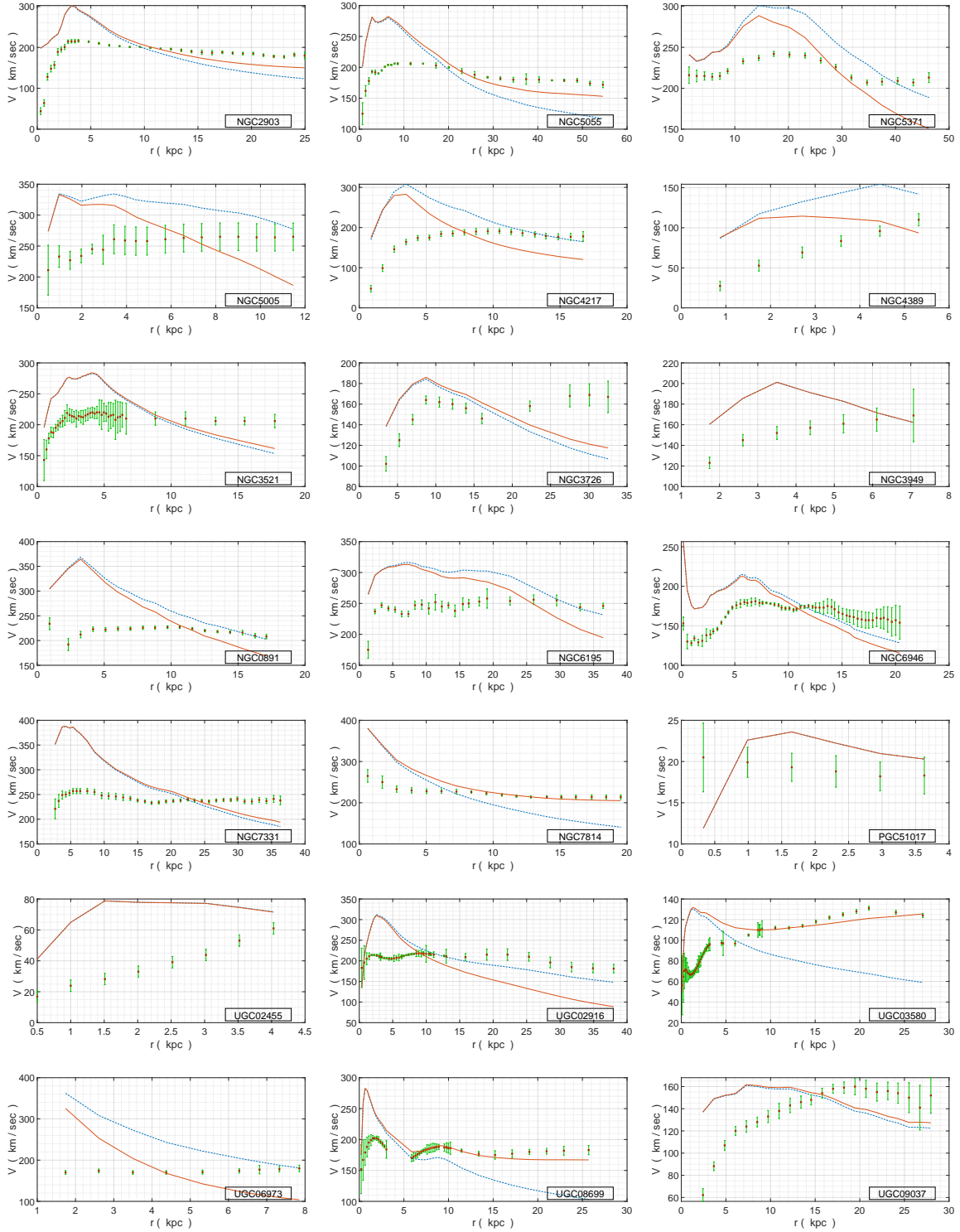


Figure 6. The graph displays the radial velocity profiles of 21 SPARC galaxies, wherein the fit using Machian Gravity is not adequate. It's evident that for all these galaxies, the Keplerian velocity calculated from visible matter significantly exceeds the observed velocities, particularly at smaller radii. This indicates a potential issue in the mass modeling for these galaxies.

Galaxy	R_{\max} [kPc]	M [$10^9 M_{\odot}$]	a [10^{-9}cm/s^2]	a_N [10^{-9}cm/s^2]	λ^{-1} [kpc]	M_c [$10^9 M_{\odot}$]	a_0 [10^{-8}cm/s^2]
D512-2	3.83	0.42	1.09	0.40	1.58	5.53	3.10
D564-8	3.07	0.08	0.66	0.11	2.57	15.42	3.25
D631-7	7.19	0.66	1.48	0.18	5.28	131.71	6.59
DDO064	2.98	0.55	2.39	0.86	1.46	10.97	7.14
DDO154	5.92	0.39	1.13	0.16	2.98	61.78	9.70
DDO161	13.37	2.98	1.06	0.23	13.26	595.51	4.72
DDO168	4.12	0.75	2.13	0.62	4.48	150.35	10.45
DDO170	12.33	2.42	1.02	0.22	4.75	68.11	4.21
ESO079-G014	16.67	66.17	6.16	3.32	13.70	753.17	5.59
ESO116-G012	9.86	7.53	4.12	1.08	9.16	872.42	14.50
ESO444-G084	4.44	0.29	2.87	0.21	1.61	58.11	31.28
ESO563-G021	42.41	382.57	7.44	2.96	33.40	8204.61	10.25
F561-1	9.66	7.41	0.85	1.11	4.60	3.19	0.21
F563-1	20.10	8.11	1.81	0.28	3.80	362.36	34.99
F563-V1	7.87	1.74	0.31	0.39	3.65	1.04	0.11
F563-V2	10.47	7.29	4.31	0.93	1.99	141.67	49.82
F565-V2	8.80	2.22	2.54	0.40	3.78	171.20	16.73
F567-2	9.59	3.74	0.92	0.57	2.41	10.55	2.54
F568-1	13.23	14.59	4.94	1.16	2.86	235.09	39.95
F568-3	17.98	16.38	2.60	0.71	7.10	290.83	8.03
F568-V1	17.63	9.82	2.56	0.44	2.65	198.94	39.44
F571-8	15.55	11.57	4.32	0.67	14.18	2313.13	16.04
F571-V1	13.59	4.85	1.68	0.37	6.72	227.82	7.02
F574-1	12.60	10.02	2.56	0.88	3.54	103.07	11.44
F574-2	10.83	5.32	0.48	0.63	7.53	0.52	0.01
F579-V1	15.16	18.09	2.78	1.10	1.54	60.60	35.55
F583-1	16.26	7.02	1.47	0.37	3.39	130.73	15.83
F583-4	7.29	2.71	2.17	0.71	4.66	59.85	3.84
IC2574	10.23	3.12	1.44	0.42	13.98	624.26	4.45
IC4202	25.90	234.65	7.63	4.88	130.72	46898.50	3.83
KK98-251	3.13	0.33	1.21	0.47	3.34	21.05	2.63

Galaxy	R_{\max} [kPc]	M [$10^9 M_{\odot}$]	a [10^{-9}cm/s^2]	a_N [10^{-9}cm/s^2]	λ^{-1} [kpc]	M_c [$10^9 M_{\odot}$]	a_0 [10^{-8}cm/s^2]
NGC0024	11.27	5.31	3.48	0.58	2.84	143.87	24.89
NGC0055	13.50	10.78	1.80	0.82	11.15	313.43	3.52
NGC0100	9.62	4.65	2.80	0.70	11.95	928.87	9.07
NGC0247	14.54	12.12	2.55	0.80	3.15	51.92	7.29
NGC0289	71.12	119.64	1.24	0.33	39.85	4725.59	4.15
NGC0300	11.80	4.69	2.40	0.47	8.06	521.33	11.19
NGC0801	59.82	410.36	2.53	1.60	256.86	82053.40	1.73
NGC0891	17.11	163.36	8.19	7.78	0.72	72.81	198.36
NGC1003	30.24	16.76	1.42	0.26	23.36	3351.63	8.56
NGC1090	30.09	98.06	2.76	1.51	76.59	19604.74	4.66
NGC1705	6.00	0.81	2.76	0.31	1.97	76.08	27.20
NGC2366	6.06	1.22	1.30	0.46	4.08	54.90	4.60
NGC2403	20.87	17.97	2.79	0.57	18.63	3547.42	14.24
NGC2683	34.62	84.96	2.13	0.99	77.75	16973.95	3.91
NGC2841	63.64	269.62	4.40	0.93	36.33	14462.51	15.27
NGC2903	24.96	88.50	4.21	1.98	86.84	17694.20	3.27
NGC2915	10.04	1.57	2.41	0.22	3.33	259.62	32.56
NGC2955	35.43	391.83	4.71	4.35	1.32	46.46	36.94
NGC2976	2.27	3.33	10.39	9.02	8.46	0.00	0.00
NGC2998	42.28	207.16	3.16	1.62	91.76	41412.75	6.85
NGC3109	6.45	0.80	2.28	0.27	3.61	160.70	17.15
NGC3198	44.08	62.38	1.63	0.45	49.70	12473.53	7.04
NGC3521	17.74	96.95	7.75	4.29	0.94	20.91	32.80
NGC3726	32.52	86.41	2.78	1.14	166.05	17246.44	0.87
NGC3741	7.00	0.32	1.23	0.09	2.38	63.48	15.65
NGC3769	37.16	27.49	1.11	0.28	37.24	5495.73	5.52
NGC3877	11.35	97.43	8.15	10.54	6.54	8.84	0.29
NGC3893	19.05	71.81	4.74	2.76	62.51	14355.69	5.12
NGC3917	14.86	30.48	4.09	1.92	8.54	217.86	4.16
NGC3949	7.07	43.18	13.09	12.04	0.05	9.25	5303.97
NGC3953	15.68	179.59	9.55	10.18	17.46	0.00	0.00

Galaxy	R_{\max} [kPc]	M [$10^9 M_{\odot}$]	a [10^{-9}cm/s^2]	a_N [10^{-9}cm/s^2]	λ^{-1} [kpc]	M_c [$10^9 M_{\odot}$]	a_0 [10^{-8}cm/s^2]
NGC3972	8.72	19.15	6.67	3.51	11.19	475.55	5.30
NGC3992	46.02	266.08	3.96	1.75	74.07	29852.53	7.58
NGC4010	10.47	22.58	4.61	2.87	31.09	4510.52	6.50
NGC4013	31.01	88.74	3.02	1.29	69.58	17742.05	5.11
NGC4051	12.19	85.38	6.22	8.01	8.35	0.00	0.00
NGC4068	2.33	0.49	2.44	1.26	7.31	98.08	2.56
NGC4085	6.20	28.82	9.67	10.45	4.56	0.00	0.00
NGC4088	21.48	128.65	4.57	3.89	1.66	43.12	21.77
NGC4100	22.76	69.03	3.60	1.86	51.38	13799.18	7.29
NGC4138	18.58	49.38	3.92	1.99	56.05	9849.35	4.37
NGC4157	29.61	122.32	3.75	1.94	147.53	24433.07	1.56
NGC4183	21.02	18.26	1.97	0.58	6.82	172.00	5.15
NGC4214	5.63	1.45	3.74	0.64	4.36	289.82	21.21
NGC4217	16.72	105.49	6.14	5.26	0.71	22.92	63.48
NGC4389	5.32	24.92	7.37	12.27	0.04	0.78	682.67
NGC4559	20.97	33.70	2.19	1.07	43.36	6733.50	4.99
NGC5005	11.47	205.21	19.84	21.74	0.25	22.17	510.66
NGC5033	44.59	138.51	2.79	0.97	31.64	4158.18	5.79
NGC5055	54.59	173.80	1.76	0.81	0.58	52.09	215.97
NGC5371	46.24	382.69	3.18	2.49	8.58	168.31	3.18
NGC5585	10.96	5.79	2.36	0.67	13.37	1157.39	9.03
NGC5907	50.33	232.78	2.95	1.28	101.11	46544.66	6.34
NGC5985	34.72	293.02	7.58	3.39	6.08	916.09	34.53
NGC6015	29.23	43.14	2.56	0.70	35.62	8624.61	9.48
NGC6195	36.43	454.27	5.38	4.77	33.66	0.00	0.00
NGC6503	23.50	16.55	1.82	0.42	21.32	2799.00	8.58
NGC6674	72.41	259.05	2.62	0.69	76.15	37632.00	9.05
NGC6789	0.71	0.10	16.65	2.73	0.67	19.72	61.78
NGC6946	20.40	78.10	3.77	2.62	14.22	0.00	0.00
NGC7331	36.31	288.33	5.06	3.05	208.40	18463.89	0.59
NGC7793	7.87	9.95	3.39	2.24	23.59	1984.28	4.97
NGC7814	19.53	90.13	7.60	3.29	41.34	18021.00	14.69

Galaxy	R_{\max} [kPc]	M [$10^9 M_{\odot}$]	a [10^{-9}cm/s^2]	a_N [10^{-9}cm/s^2]	λ^{-1} [kpc]	M_c [$10^9 M_{\odot}$]	a_0 [10^{-8}cm/s^2]
PGC51017	3.63	0.35	0.30	0.37	0.15	0.11	6.73
UGC00128	53.75	27.94	0.94	0.13	10.79	816.53	9.77
UGC00191	9.98	5.01	2.28	0.70	3.12	54.62	7.81
UGC00634	18.01	8.86	2.08	0.38	9.71	732.70	10.83
UGC00731	10.91	3.66	1.62	0.43	1.15	42.85	45.15
UGC00891	7.39	1.23	1.78	0.31	6.22	245.66	8.85
UGC01230	36.54	21.60	0.94	0.23	5.10	261.11	13.99
UGC02023	3.78	1.51	2.96	1.47	11.41	301.30	3.23
UGC02259	8.14	3.38	3.22	0.71	1.89	49.72	19.43
UGC02455	4.03	4.82	2.99	4.14	0.04	0.15	136.45
UGC02487	80.38	567.89	4.47	1.23	30.89	8618.41	12.58
UGC02885	74.07	589.68	3.89	1.50	126.90	117864.77	10.20
UGC02916	38.00	194.18	2.79	1.87	0.21	30.52	977.33
UGC02953	62.39	283.26	3.84	1.01	84.81	56638.51	10.98
UGC03205	40.04	137.92	3.92	1.20	63.17	27577.96	9.63
UGC03546	29.23	115.13	4.13	1.88	108.22	23018.33	2.74
UGC03580	27.06	21.90	1.84	0.42	30.07	4379.50	6.75
UGC04278	6.69	4.12	4.17	1.28	7.19	625.24	16.86
UGC04305	5.52	1.88	0.64	0.86	1.51	0.67	0.41
UGC04325	5.59	3.80	4.85	1.69	1.02	26.19	35.26
UGC04483	1.21	0.06	1.57	0.55	0.74	1.37	3.51
UGC04499	8.18	4.07	2.19	0.85	4.52	66.63	4.54
UGC05005	28.61	14.56	1.11	0.25	21.20	1808.47	5.61
UGC05253	53.29	221.94	2.89	1.09	110.38	44376.56	5.08
UGC05414	4.11	1.65	2.97	1.36	8.30	328.50	6.64
UGC05716	12.37	2.84	1.46	0.26	3.47	89.78	10.42
UGC05721	6.74	1.49	3.04	0.46	1.80	74.24	31.86
UGC05750	22.85	11.01	0.88	0.29	6.92	124.04	3.61
UGC05764	3.62	0.43	2.23	0.46	0.61	11.33	42.90
UGC05829	6.91	2.58	2.21	0.75	2.19	22.14	6.41
UGC05918	4.46	0.55	1.44	0.39	0.98	6.87	9.90

Galaxy	R_{\max} [kPc]	M [$10^9 M_{\odot}$]	a [10^{-9}cm/s^2]	a_N [10^{-9}cm/s^2]	λ^{-1} [kpc]	M_c [$10^9 M_{\odot}$]	a_0 [10^{-8}cm/s^2]
UGC05986	9.41	6.85	3.94	1.08	7.24	604.94	16.07
UGC05999	16.22	12.55	2.00	0.66	8.66	323.52	6.01
UGC06399	7.85	4.23	3.17	0.96	4.01	99.27	8.60
UGC06446	10.22	3.71	2.03	0.50	2.13	60.44	18.55
UGC06614	64.59	196.51	2.09	0.66	111.37	39284.25	4.41
UGC06628	7.69	5.67	0.75	1.34	4.35	0.11	0.01
UGC06667	7.85	2.14	3.03	0.48	1.39	76.81	55.65
UGC06786	34.05	87.12	4.24	1.05	33.32	17420.10	21.87
UGC06787	37.19	122.13	5.67	1.23	42.35	24420.42	18.97
UGC06818	6.98	2.67	2.57	0.76	11.61	533.43	5.51
UGC06917	10.47	12.13	3.81	1.54	6.32	195.35	6.82
UGC06923	5.16	4.37	4.13	2.29	12.67	870.12	7.55
UGC06930	16.61	16.50	2.28	0.83	6.04	137.85	5.26
UGC06973	7.85	59.84	13.37	13.53	0.05	9.41	5023.91
UGC06983	15.68	11.69	2.46	0.66	4.79	177.50	10.79
UGC07089	9.16	5.89	2.21	0.98	20.40	1174.06	3.93
UGC07125	18.68	8.13	0.73	0.32	8.81	61.64	1.11
UGC07151	5.50	3.95	3.42	1.82	2.74	22.79	4.23
UGC07232	0.82	0.14	7.65	2.98	1.75	28.68	13.08
UGC07261	6.67	3.29	2.81	1.03	3.34	45.09	5.63
UGC07323	5.82	6.13	4.08	2.52	17.65	1221.89	5.47
UGC07399	6.13	2.30	5.94	0.85	1.90	119.62	45.98
UGC07524	10.69	6.62	1.89	0.81	3.06	48.60	7.24
UGC07559	2.53	0.30	1.32	0.65	5.13	59.86	3.17
UGC07577	1.69	0.09	0.61	0.43	14.16	0.01	0.00
UGC07603	4.11	0.70	3.23	0.58	3.31	139.55	17.76
UGC07608	4.78	0.94	3.26	0.57	2.00	58.38	20.34
UGC07690	4.13	1.41	2.45	1.16	2.19	12.45	3.60
UGC07866	2.32	0.26	1.53	0.66	1.54	3.33	1.95
UGC08286	8.04	2.70	2.86	0.58	2.33	67.46	17.39
UGC08490	10.15	2.24	1.92	0.30	3.01	105.57	16.21
UGC08550	5.36	0.91	2.00	0.44	2.08	33.62	10.81

Galaxy	R_{\max} [kPc]	M [$10^9 M_{\odot}$]	a [10^{-9}cm/s^2]	a_N [10^{-9}cm/s^2]	λ^{-1} [kpc]	M_c [$10^9 M_{\odot}$]	a_0 [10^{-8}cm/s^2]
UGC08699	25.70	63.39	4.22	1.34	44.11	12673.65	9.08
UGC08837	4.20	1.16	1.78	0.92	11.63	232.90	2.40
UGC09037	27.96	97.50	2.68	1.74	255.33	19482.38	0.42
UGC09133	108.31	368.98	1.57	0.44	98.21	33142.66	4.79
UGC09992	3.89	0.72	0.98	0.66	1.80	2.25	0.97
UGC10310	7.74	3.98	2.24	0.93	2.19	24.31	7.09
UGC11455	41.93	435.07	5.47	3.45	268.62	86981.64	1.68
UGC11557	10.56	18.09	2.19	2.26	7.81	0.00	0.00
UGC11820	15.82	5.67	1.46	0.32	6.58	178.47	5.74
UGC11914	9.83	159.33	30.67	22.98	12.92	0.00	0.00
UGC12506	49.99	236.81	3.28	1.32	11.43	1452.11	15.48
UGC12632	10.66	4.22	1.62	0.52	2.55	43.43	9.31
UGC12732	15.40	8.60	2.02	0.51	4.44	147.59	10.45
UGCA281	1.08	0.09	2.61	1.13	0.92	2.35	3.85
UGCA442	6.33	0.58	1.63	0.20	3.60	115.75	12.45
UGCA444	2.62	0.13	1.81	0.27	1.02	4.74	6.32

Table 1. The table provides information on various parameters for each SPARC galaxy, including the radius of the last velocity data point (R_{\max}), mass (M), centripetal acceleration (a) at the last data point, centripetal acceleration calculated using Newtonian mechanics at the last velocity data point, best fit value of λ^{-1} , M_c , and the derived value of $a_0 = \frac{GM_c}{\lambda^{-2}}$. It's evident that the value of a_0 varies significantly among different galaxies, indicating that a uniform a_0 may not be sufficient to adequately explain the velocity profiles of all galaxies.